CJE

RESEARCH ARTICLE

Optical Space Time Pulse Position Modulation over Exponential Weibull Turbulence Channel

Yue ZHANG[1], Huiqin WANG[1], Xuemei MA[2], Minghua CAO[1], and Qingbin PENG[1]

1. *School of Computer and Communication, Lanzhou University of Technology, Lanzhou 730050, China*
2. *School of Foreign Languages, Lanzhou University of Technology, Lanzhou 730050, China*

Corresponding author: Huiqin WANG, Email: whq1222@lut.edu.cn

Abstract — An optical space time pulse position modulation (OSTPPM) scheme is proposed to satisfy the communication requirement of high transmission rate and better reliability. For the OSTPPM scheme, an improved threshold judgment-based orthogonal matching pursuit (IT-OMP) algorithm with low-complexity and near optimal performance is proposed. The average bit error rate of OSTPPM-IT-OMP scheme is investigated over the exponential Weibull channel, and its analytical expression is verified via Monte Carlo simulation. With the same simulation parameters, the signal to noise ratio of (4,4,2)-OSTPPM-IT-OMP is respectively 3.75 dB and 8.5 dB better than that of spatial pulse position modulation (SPPM) scheme and generalized spatial pulse position modulation (GSPPM) scheme at a bit error rate of 1×10^{-3}. With the same transmission bits per symbol, the computational complexity of (3,4,2)-OSTPPM-IT-OMP scheme is reduced by 90.47% and 75.4% compared with (16,4,2)-SPPM and (5,4,2)-GSPPM schemes, respectively.

Keywords — Optical wireless communication, Optical spatial modulation, Pulse position modulation, Compressed sensing.

I. Introduction

With the growing demand for data service, there are higher requirements of transmission rate and reliability of optical wireless communication system [1]. Thus, optical multiple input multiple output (OMIMO) technology has sparked interest in this field due to its high capacity and reliability [2]. Optical spatial modulation (OSM) is a promising OMIMO technology where the antenna index transfers additional information [3], [4]. As only one antenna is activated in a period, the inter-channel interference and inter-antenna synchronization are efficiently avoided [5].

It is worth noting that optical spatial pulse position amplitude modulation (SPPAM), optical spatial pulse position modulation (SPPM) and adaptive closed-loop SPPM scheme are developed in [6]–[9]. However, since only one laser is activated at intervals in OSM schemes, their transmission rates are limited. To increase the transmission rate of OSM, several generalized optical spatial modulation (GOSM) schemes, such as optical generalized spatial pulse position modulation (GSPPM), optical generalized

spatial pulse amplitude modulation (GSPAM) and power efficient optical GSPAM are proposed in [10]–[12]. In GOSM schemes, a part of lasers are activated at intervals simultaneously, and modulation symbols are mapped on activated lasers to transfer information. In order to further enhance the overall transmission capacity, bandwidth efficiency and bit error rate (BER) performance, hybrid diversity SPPM scheme and wavelength-division multiplexing with spatial division multiplexing and hybrid M-ary PPM advanced optical modulation techniques are proposed in [13]–[17]. Then, the combined effects of atmospheric turbulence, geometric spreading, inter-channel crosstalk and other factors on performance of the proposed schemes are investigated. It is important to research the performance of orthogonal frequency division multiplexing (OFDM) [18] and asymmetrically clipped DC-biased optical OFDM [19] system, which is support to improve the transmission rate and spectral efficiency. However, it is difficult to accurately estimate channel state information (CSI) in actual communication systems, differential optical spatial modulation schemes are proposed

in [20], [21] to avoid the estimation of CSI. Reference [22] indicates that the transmission rate of GOSM is enhanced at the expense of BER performance. Thus, we need to seek a new modulation scheme with higher transmission rate and better BER performance.

In addition, the decoding algorithm of all the aforementioned OSM and GOSM schemes at the receiver adopts maximum likelihood sequence detection (MLSD). Although MLSD achieves the optimal performance, its application is limited due to its higher computational complexity. Then, in [23], [24], orthogonal matching pursuit (OMP) decoding algorithm and k-means clustering decoding algorithm are used in optical SPPM scheme to reduce the computational complexity. Moreover, an improved compressed sensing based on threshold judgment decoding algorithm is proposed for optical space-time shift-keying (OSTSK) scheme in [25]. When the appropriate threshold is selected, the BER performance of the proposed algorithm and its computational complexity can reach a compromise. However, without using symbols constellation, the transmission rate of OSTSK is limited. The average bit error rate (ABER) expression of OSTSK-MLSD over Gamma-Gamma channel is derived. Considering the error propagation and noise amplification effects, a deep neural network-aided detection for generalized optical quadrature spatial modulation is proposed to improve BER performance [26]. Therefore, finding a decoding algorithm with better BER performance and low-complexity is key to the practical application of OSM schemes.

All the above GOSM schemes have enhanced the transmission rate at the cost of BER performance loss, and their decoding algorithms are adopted MLSD with higher computational complexity, which limit their practical application. Concerning this issue, in this paper, we introduce linear dispersion code and pulse position modulation (PPM) into OSM, and propose an optical space time pulse position modulation (OSTPPM) to improve the BER performance. A low-complexity decoding algorithm for OSTPPM scheme is proposed, which promotes the practical application of the considered scheme. In spatial domain, space time dispersion matrix is designed to represent the combination of activated laser indices, improving BER performance of the system. In signal domain, multiplexing technology is used to transmit the different PPM symbols on all the activated lasers, maximizing the transmission rate of scheme. Furthermore, considering the sparsity of the transmitted signal in OSTPPM scheme, we propose the improved orthogonal matching pursuit based on threshold judgment (IT-OMP) decoding algorithm, which has better BER performance near optimal detector and significant low-complexity. In the end, the analytical expression of average bit error rate for OSTPPM-IT-OMP system under exponential Weibull (EW) turbulence channel is derived.

The rest of this paper is organized as follows: In Section II, the system model for OSTPPM-IT-OMP is introduced. In Section III, the analytical expression of the average bit error rate of OSTPPM-IT-OMP is derived. In Section IV, simulation results and analysis are expressed, where the Monte Carlo method is used to investigate the performance of our proposal. Finally, conclusions are given in Section V.

II. System Model

The model of $N_t \times N_r$ OSTPPM system is shown in Figure 1, where N_t and N_r are the number of lasers and photo-detectors (PDs), respectively. At the transmitter, the incoming random bits are divided into groups of l_N bits. The bit block l_N is partitioned into two segments. The first segment containing $\lfloor \log_2(N_t!) \rfloor$ bits is used to select the combination of activated laser indices in spatial domain, where $\lfloor \cdot \rfloor$ denotes the floor function. In other words, the spatial constellation point is represented by an unique orthogonal space time dispersion matrix $\boldsymbol{x}_s$. The other segment with $N_t \log_2 L$ bits is mapped to N_t L-PPM symbols in signal domain, in which L stands for PPM order. The modulation symbol is $\Im = (\boldsymbol{x}_{p_1}, \ldots, \boldsymbol{x}_{p_u}, \ldots, \boldsymbol{x}_{p_{N_t}} | 1 \le u \le N_t)$, in which $\boldsymbol{x}_{p_u}$ contains $\log_2 L$ bits. In this way, the transmission bits per symbol (TBS) and spectral efficiency of OSTPPM scheme are respectively $R = \lfloor \log_2(N_t!) \rfloor + N_t \log_2 L$ bpcu (bits per channel use) and $\upsilon = [\lfloor \log_2(N_t!) \rfloor + N_t \log_2 L]/(N_t L)$ bits/s/Hz. The transmitted signal composed of $\boldsymbol{x}_s$ and PPM symbol is received by the PDs at the receiver after passing through the atmospheric turbulence (AT) channel. The IT-OMP algorithm is proposed to detect estimated signal. Then, estimated signal is demodulated to recover the original bit sequences.

1. Mapping rules
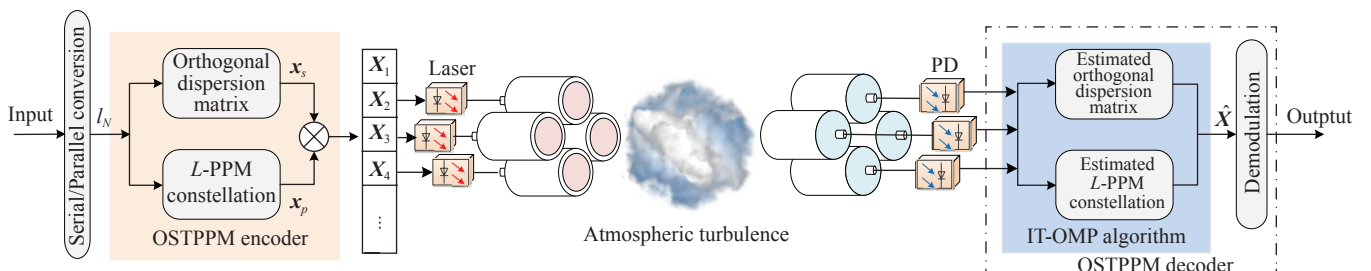
The OSTPPM scheme includes both spatial domain

Figure 1 OSTPPM-IT-OMP system model.

mapping and signal domain mapping. In spatial domain, $\boldsymbol{x}_s$ is generated from N_t laser indices according to the criterion of rank maximization of the space time dispersion matrix. Then, $\boldsymbol{x}_s$ is orthogonal, and there is only one nonzero element in each column and row in $\boldsymbol{x}_s$. Thus, it can be expressed as $\boldsymbol{x}_s = \left[\boldsymbol{x}_{s_1}, \ldots, \boldsymbol{x}_{s_i}, \ldots, \boldsymbol{x}_{s_{N_t}}\right]$, $1 \leq i \leq N_t$, where $\boldsymbol{x}_{s_i} = \left[0, \ldots, 0, \underset{\underset{a_j}{\uparrow}}{1}, 0, \ldots, 0\right]^{\mathrm{T}}$, a_j $(1 \leq j \leq N_t)$ is the activated laser index.

In signal domain, a PPM symbol period is divided into L time slots. The PPM symbol consists of "on" and "off" time slots, hence it can be expressed as $\boldsymbol{x}_{p_u} = [0, \ldots, A_m, \ldots, 0]$, where d_e $(1 \leq e \leq L)$ denotes the position of "on" slot, A_m denotes light intensity in an time

slot. Moreover, multiplexing technology is used in signal domain, that is, different L-PPM symbols are mapped on each activated laser. Thus, the mapping matrix is expressed as $\boldsymbol{x}_p = \begin{bmatrix} \boldsymbol{x}_{p_1}, \ldots, \boldsymbol{O}, \ldots, \boldsymbol{O} \\ \boldsymbol{O}, \ldots, \boldsymbol{x}_{p_u}, \ldots, \boldsymbol{O} \\ \boldsymbol{O}, \ldots, \boldsymbol{O}, \ldots, \boldsymbol{x}_{p_{N_t}} \end{bmatrix}$, $\boldsymbol{O} = [0, \ldots, 0]$ is the $1 \times L$ dimensional zero vector.

Therefore, the transmitted signal $\boldsymbol{X}$ is generated by multiplying $\boldsymbol{x}_s$ and $\boldsymbol{x}_p$ as

$$\boldsymbol{X} = \boldsymbol{x}_s \cdot \boldsymbol{x}_p \tag{1}$$

where $\boldsymbol{X}$ is expanded to an $N_t \times (N_t L)$ dimensional matrix.

Consider an OSTPPM scheme with $N_t = 3$ and $L = 2$, in which the TBS is 5 bpcu. The mapping rules are represented in Table 1.

Table 1 Mapping rules table of OSTPPM

Bit sequences	$\boldsymbol{x}_s$	$\boldsymbol{x}_{p_1}$	$\boldsymbol{x}_{p_2}$	$\boldsymbol{x}_{p_3}$	$\boldsymbol{X}$
00000	$\begin{bmatrix} 1 & 0 & 0 \\ 0 & 1 & 0 \\ 0 & 0 & 1 \end{bmatrix}$	$[A_m, 0]$	$[A_m, 0]$	$[A_m, 0]$	$\begin{bmatrix} A_m & 0 & 0 & 0 & 0 & 0 \\ 0 & 0 & A_m & 0 & 0 & 0 \\ 0 & 0 & 0 & 0 & A_m & 0 \end{bmatrix}$
00001	$\begin{bmatrix} 1 & 0 & 0 \\ 0 & 1 & 0 \\ 0 & 0 & 1 \end{bmatrix}$	$[A_m, 0]$	$[A_m, 0]$	$[0, A_m]$	$\begin{bmatrix} A_m & 0 & 0 & 0 & 0 & 0 \\ 0 & 0 & A_m & 0 & 0 & 0 \\ 0 & 0 & 0 & 0 & 0 & A_m \end{bmatrix}$
00010	$\begin{bmatrix} 1 & 0 & 0 \\ 0 & 1 & 0 \\ 0 & 0 & 1 \end{bmatrix}$	$[A_m, 0]$	$[0, A_m]$	$[A_m, 0]$	$\begin{bmatrix} A_m & 0 & 0 & 0 & 0 & 0 \\ 0 & 0 & 0 & A_m & 0 & 0 \\ 0 & 0 & 0 & 0 & A_m & 0 \end{bmatrix}$
00011	$\begin{bmatrix} 1 & 0 & 0 \\ 0 & 1 & 0 \\ 0 & 0 & 1 \end{bmatrix}$	$[A_m, 0]$	$[0, A_m]$	$[0, A_m]$	$\begin{bmatrix} A_m & 0 & 0 & 0 & 0 & 0 \\ 0 & 0 & 0 & A_m & 0 & 0 \\ 0 & 0 & 0 & 0 & 0 & A_m \end{bmatrix}$
$\vdots$	$\vdots$	$\vdots$	$\vdots$	$\vdots$	$\vdots$
01000	$\begin{bmatrix} 1 & 0 & 0 \\ 0 & 0 & 1 \\ 0 & 1 & 0 \end{bmatrix}$	$[A_m, 0]$	$[A_m, 0]$	$[A_m, 0]$	$\begin{bmatrix} A_m & 0 & 0 & 0 & 0 & 0 \\ 0 & 0 & 0 & A_m & 0 & 0 \\ 0 & 0 & 0 & 0 & A_m & 0 \end{bmatrix}$
01001	$\begin{bmatrix} 1 & 0 & 0 \\ 0 & 0 & 1 \\ 0 & 1 & 0 \end{bmatrix}$	$[A_m, 0]$	$[A_m, 0]$	$[0, A_m]$	$\begin{bmatrix} A_m & 0 & 0 & 0 & 0 & 0 \\ 0 & 0 & 0 & 0 & 0 & A_m \\ 0 & 0 & A_m & 0 & 0 & 0 \end{bmatrix}$
$\vdots$	$\vdots$	$\vdots$	$\vdots$	$\vdots$	$\vdots$
11111	$\begin{bmatrix} 0 & 0 & 1 \\ 0 & 1 & 0 \\ 1 & 0 & 0 \end{bmatrix}$	$[0, A_m]$	$[0, A_m]$	$[0, A_m]$	$\begin{bmatrix} 0 & 0 & 0 & 0 & 0 & A_m \\ 0 & 0 & 0 & A_m & 0 & 0 \\ 0 & A_m & 0 & 0 & 0 & 0 \end{bmatrix}$

2. Channel model

Optical signal propagation is affected by AT, which fades the signal at the receiver and deteriorates the BER performance. Due to variations in the refractive index caused by inhomogeneities in the temperature and pressure of the atmosphere, it leads to random fluctuations in both amplitude and phase of the received optical signal, resulting in degrading the BER performance [27]. Mathematically, the received signal of the OSTPPM under intensity-modulation/direct-detection (IM/DD) is [28]

$$\boldsymbol{Y} = \eta P_t \boldsymbol{H} \boldsymbol{X} + \boldsymbol{n} \tag{2}$$

where $\boldsymbol{n}$ is additive white Gauss noise with mean of e_n

and variance of σ_n^2. η is the photoelectric conversion efficiency of the PDs. P_t is the optical power. $\boldsymbol{H} \in \Re^{N_r \times N_t}$ is channel gain matrix, h of it subjected to EW distribution. EW distribution is proved to be the more suitable model to describe the weak to strong AT channel [29]. The probability density function (PDF) of h is written as

$$f(h_{kt}) = \frac{\alpha\beta}{\wp} \left(\frac{h_{kt}}{\wp}\right)^{\beta-1}$$
$$\times \exp\left[-\left(\frac{h_{kt}}{\wp}\right)^{\beta}\right] \left\{1 - \exp\left[-\left(\frac{h_{kt}}{\wp}\right)^{\beta}\right]\right\}^{\alpha-1} \tag{3}$$

where the parameters of α, β and $\wp$ are given in [29].

3. Low-complexity decoding algorithm

Utilizing the sparsity of transmitted signal, we propose a new low-complexity decoding algorithm near optimal BER performance for OSTPPM scheme, called IT-OMP algorithm. The threshold V_{th} is introduced in the algorithm to improve the BER performance as well as to realize low-complexity decoding. The algorithm flow chart is shown in Figure 2, and the algorithm is as follows.

Firstly, we initialize the residual $\boldsymbol{R}_0 = \boldsymbol{Y}$, laser indices set $\boldsymbol{\Lambda}_0 = \varnothing$ and PPM symbols set $\boldsymbol{\varphi}_0 = \varnothing$. Then, the inner product matrix is calculated as

$$\boldsymbol{\phi} = \langle \boldsymbol{Y}, \boldsymbol{H} \rangle = \boldsymbol{H}^{\mathrm{T}}\boldsymbol{Y} \qquad (4)$$

where $\boldsymbol{\phi} = [\boldsymbol{\zeta}_1, \boldsymbol{\zeta}_2, \ldots, \boldsymbol{\zeta}_{N_t L}]$ is the $N_t \times N_t L$ dimensional matrix, $\boldsymbol{\zeta}$ is the column vector in $\boldsymbol{\phi}$.

Secondly, the consecutive L columns vector in $\boldsymbol{\phi}$ are selected and sorted reversely:

$$\{\boldsymbol{y}_1, \ldots, \boldsymbol{y}_{ii}, \ldots, \boldsymbol{y}_\omega\} = \arg \mathrm{sort}\{[\boldsymbol{\zeta}_\varepsilon : \boldsymbol{\zeta}_{tL}]\} \qquad (5)$$

where ω, ε and t are variables, and $\omega < N_t L$, $1 \le \varepsilon \le (N_t - 1)L$, $1 \le t \le N_t$.

According to (5), the row and column corresponding to each candidate value $\boldsymbol{y}_{ii}$ can be extracted as $\hat{\boldsymbol{x}}_{s_{\varepsilon_{ii}}}$ and $\hat{\boldsymbol{x}}_{p_{\varepsilon_{ii}}}$. $\hat{\boldsymbol{x}}_{s_{\varepsilon_{ii}}}$ denotes the estimated activated laser index, and $\hat{\boldsymbol{x}}_{p_{\varepsilon_{ii}}}$ denotes the estimated position of "on" slot in PPM symbol. Then, laser indices set and PPM symbols set are updated to $\boldsymbol{\Lambda}_{\varepsilon_t} = \boldsymbol{\Lambda}_{\varepsilon_{t-1}} \cup \hat{\boldsymbol{x}}_{s_{\varepsilon_{ii}}}$ and $\boldsymbol{\varphi}_{\varepsilon_t} = \boldsymbol{\varphi}_{\varepsilon_{t-1}} \cup \hat{\boldsymbol{x}}_{p_{\varepsilon_{ii}}}$.

The second step is repeated N_t times until the useful information of the $N_t L$ columns in the inner product matrix is obtained.

Thirdly, the possible signal estimated in the second step is $\boldsymbol{Z} = \{\boldsymbol{POS}_{ii}|1 \le ii \le N_t L\}$, where $\boldsymbol{POS}_{ii}$ is an estimated signal consisting of $\hat{\boldsymbol{x}}_{s_{\varepsilon_{ii}}}$ and $\hat{\boldsymbol{x}}_{p_{\varepsilon_{ii}}}$. All possible estimated signals are

$$\left\{\hat{\boldsymbol{X}}_1, \hat{\boldsymbol{X}}_2, \ldots, \hat{\boldsymbol{X}}_W\right\} = \arg\min \|\boldsymbol{POS}_{ii} - \boldsymbol{X}\|_F^2 \qquad (6)$$

Fourthly, we preset a threshold V_{th} to determine the reliability of the estimated results

$$\left\|\boldsymbol{Y} - \eta P_t \boldsymbol{H}\hat{\boldsymbol{X}}_{jj}\right\|_F^2 \le V_{\mathrm{th}} \qquad (7)$$

where $1 \le jj \le W$, $V_{\mathrm{th}} = \theta N_t N_r L \sigma_n^2$, θ is a parameter utilized to balance the computational complexity and the BER performance.

If $\hat{\boldsymbol{X}}_{jj}$ satisfies (7), then $\hat{\boldsymbol{X}}_{\mathrm{final}} = \hat{\boldsymbol{X}}_{jj}$ is the final estimated result. Otherwise, the final output is expressed as

$$\hat{\boldsymbol{X}}_{\mathrm{final}} = \arg\min \left\|\boldsymbol{Y} - \eta \boldsymbol{H}\hat{\boldsymbol{X}}_{jj}\right\|_F^2 \qquad (8)$$
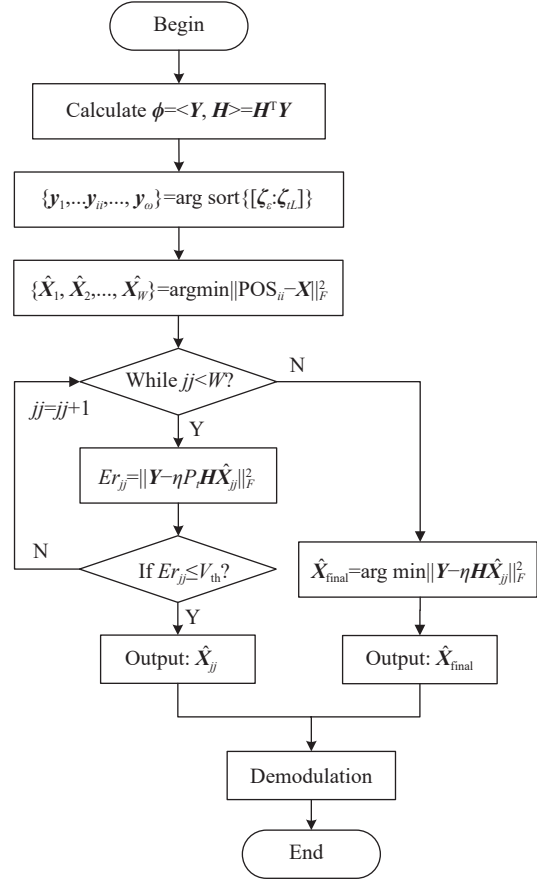

Figure 2 The IT-OMP algorithm flow chart.

Finally, $\hat{\boldsymbol{X}}_{\mathrm{final}}$ is demodulated to the corresponding bit sequence.

For IT-OMP algorithm, V_{th} is a key factor affecting system performance. Therefore, we analyze how to choose a more appropriate threshold.

The Euclidean distance of possible transmitted signal $\boldsymbol{X}_i$ and $\hat{\boldsymbol{X}}_{\mathrm{final}_i}$ is

$$\rho = \left\|\boldsymbol{Y} - \eta P_t \boldsymbol{H}\hat{\boldsymbol{X}}_{\mathrm{final}_i}\right\|_F^2 = \|\boldsymbol{n}\|_F^2, \quad \boldsymbol{X} = \hat{\boldsymbol{X}}_{\mathrm{final}_i} \qquad (9)$$

In (9), ρ/σ_n^2 follows the central chi-square distribution with freedom degree $N_r N_t L$. The probability $Pr(\rho \le V_{\mathrm{th}})$ that the signal Euclidean distance falls within the threshold is

$$Pr(\rho \le V_{\mathrm{th}}) = \int_0^{V_{\mathrm{th}}/\sigma_n^2} f_{\chi^2(N_r N_t L)}(x)\mathrm{d}x \qquad (10)$$

When $Pr(\rho \le V_{\mathrm{th}}) > 0.9$ is satisfied, the computational complexity of the proposed algorithm is low [30]. As $V_{\mathrm{th}}/\sigma_n^2 = \theta N_r N_t L$, $Pr(\rho \le V_{\mathrm{th}})$ is only related to $N_r N_t L$ and θ.

In addition, the computational complexities of the IT-OMP and MLSD algorithms are given as

$$\begin{aligned} C_{\mathrm{IT-OMP}} &= 2N_r N_t^2 L - N_t^2 L + N_r N_t \\ &\quad + \left(2N_r N_t^2 L + 2N_r N_t L - 1\right)\gamma \end{aligned} \qquad (11)$$

and

$$C_{\text{MLSD}} = 2^{\lfloor \log_2(N_t!) \rfloor + N_t \log_2 L} \left(2N_r N_t^2 L + 2N_r N_t L - 1 \right) \tag{12}$$

where γ denotes the calculation times less than V_{th}.

Therefore, the variance ratio of computational complexity of OSTPPM-IT-OMP is given as

$$V_R = \frac{C_{\text{MLSD}} - C_{\text{IT-OMP}}}{C_{\text{MLSD}}} \times 100\% \tag{13}$$

III. Performance Analysis

In this section, the ABER of the OSTPPM-IT-OMP system is analyzed under the EW turbulence channel. The Euclidean distance between possible transmitted signal $\boldsymbol{X}_i$ and misestimated result $\hat{\boldsymbol{X}}_{\text{final}_i}$ is

$$\rho_e = \left\| \boldsymbol{H} \left(\hat{\boldsymbol{X}}_{\text{final}_i} - \boldsymbol{X}_i \right) + \boldsymbol{n} \right\|_F^2, \quad \boldsymbol{X}_i \neq \hat{\boldsymbol{X}}_{\text{final}_i} \tag{14}$$

The ABER of the OSTPPM-IT-OMP system is divided into two parts, such as $\text{ABER}_{\rho_e \leq V_{\text{th}}}$ and $\text{ABER}_{\rho_e > V_{\text{th}}}$. The former is the ABER that the Euclidean distance between $\hat{\boldsymbol{X}}_{\text{final}_i}$ and $\boldsymbol{X}_i$ falls within V_{th}. The latter is the ABER that the Euclidean distance between $\hat{\boldsymbol{X}}_{\text{final}_i}$ and $\boldsymbol{X}_i$ falls outside V_{th}. The $\text{ABER}_{\rho_e > V_{\text{th}}}$ is used to select the signal with the smallest Euclidean distance of all signals as the $\hat{\boldsymbol{X}}_{\text{final}_i}$, and its ABER can be approximated as the ABER with MLSD.

Thus, the ABER of OSTPPM-IT-OMP can be obtained as

$$\text{ABER} = \text{ABER}_{\rho_e \leq V_{\text{th}}} + \text{ABER}_{\text{MLSD}} \tag{15}$$

A tight upper bound of the $\text{ABER}_{\rho_e \leq V_{\text{th}}}$, which is based on the union bound approach [11], can be obtained by summing the average pair-wise error probabilities (APEPs).

The $\text{ABER}_{\rho_e \leq V_{\text{th}}}$ is

$$\text{ABER}_{\rho_e \leq V_{\text{th}}} = \frac{1}{R2^R} \sum \sum d_H \left(\boldsymbol{X}_i, \hat{\boldsymbol{X}}_{\text{final}_i} \right) \\ \times \text{APEP} \left(\boldsymbol{X}_i \to \hat{\boldsymbol{X}}_{\text{final}_i} \,|\, \rho_e \leq V_{\text{th}} \right) \tag{16}$$

where $d_H \left(\boldsymbol{X}_i, \hat{\boldsymbol{X}}_{\text{final}_i} \right)$ is the hamming distance between $\boldsymbol{X}_i$ and $\hat{\boldsymbol{X}}_{\text{final}_i}$, $\text{APEP} \left(\boldsymbol{X}_i \to \hat{\boldsymbol{X}}_{\text{final}_i} \,|\, \rho_e \leq V_{\text{th}} \right)$ can be given by

$$\text{APEP} \left(\boldsymbol{X}_i \to \hat{\boldsymbol{X}}_{\text{final}_i} \,|\, \rho_e \leq V_{\text{th}} \right) \\ = Pr \left(\rho_e \leq V_{\text{th}} \right) \times \bar{P}r \left(\hat{\boldsymbol{X}}_{\text{final}_i} \neq \boldsymbol{X}_i \,|\, \rho_e \leq V_{\text{th}} \right) \tag{17}$$

where $\bar{P}r \left(\hat{\boldsymbol{X}}_{\text{final}_i} \neq \boldsymbol{X}_i \,|\, \rho_e \leq V_{\text{th}} \right)$ is the average probability of $\hat{\boldsymbol{X}}_{\text{final}_i}$ being misestimated within the threshold. Further, it can be described as

$$\bar{P}r \left(\hat{\boldsymbol{X}}_{\text{final}} \neq \boldsymbol{X}_i \,|\, \rho_e \leq V_{\text{th}} \right) \\ = \bar{P}r \left(\left\| \boldsymbol{Y} - \eta P_t \boldsymbol{H} \hat{\boldsymbol{X}}_{\text{final}} \right\|^2 \geq \left\| \boldsymbol{Y} - \eta P_t \boldsymbol{H} \boldsymbol{X}_i \right\|^2 \right) \\ = \bar{P}r \left(\eta P_t \left\| \boldsymbol{H} \hat{\boldsymbol{X}}_{\text{final}} \right\|^2 - 2 trace \left(\boldsymbol{Y}^{\text{T}} \boldsymbol{H} \hat{\boldsymbol{X}}_{\text{final}} \right) \right. \\ \left. \geq \eta P_t \| \boldsymbol{H} \boldsymbol{X}_i \|^2 - 2 \text{trace} \left(\boldsymbol{Y}^{\text{T}} \boldsymbol{H} \boldsymbol{X}_i \right) \right) \tag{18}$$

Since $\boldsymbol{X}_i$ is sparse, then $\boldsymbol{H} \boldsymbol{X}_i$ and $\boldsymbol{H} \hat{\boldsymbol{X}}_{\text{final}_i}$ in (18) can be simplified to $\boldsymbol{H} \boldsymbol{X}_i = A_m \boldsymbol{G}_i$ and $\boldsymbol{H} \hat{\boldsymbol{X}}_{\text{final}_i} = A_m \boldsymbol{G}_j$. Equation (18) can be obtained as

$$\bar{P}r \left(\hat{\boldsymbol{X}}_{\text{final}} \neq \boldsymbol{X}_i \,|\, \rho_e \leq V_{\text{th}} \right) \\ = \bar{P}r \left(\frac{2A_m}{\eta P_t} \boldsymbol{Y}^{\text{T}} \left(\boldsymbol{G}_j - \boldsymbol{G}_i \right) \geq \| \boldsymbol{G}_j \|^2 - \| \boldsymbol{G}_i \|^2 \right) \tag{19}$$

where $\boldsymbol{G}_i = [\boldsymbol{g}_1, \ldots, \boldsymbol{g}_{N_t L}]$ is the $N_r \times N_t L$ matrix.

Substitute (2) into (19), we have

$$\bar{P}r \left(\hat{\boldsymbol{X}}_{\text{final}_i} \neq \boldsymbol{X}_i \,|\, \rho_e \leq V_{\text{th}} \right) \\ = \bar{P}r \left(\frac{2A_m}{\eta P_t} \boldsymbol{n}^{\text{T}} \left(\boldsymbol{G}_j - \boldsymbol{G}_i \right) \geq \| \boldsymbol{G}_j - \boldsymbol{G}_i \|^2 \right) \tag{20}$$

Define $\Delta = (2A_m / \eta P_t) \boldsymbol{n}^{\text{T}} \left(\boldsymbol{G}_j - \boldsymbol{G}_i \right)$, and Δ obeys Gaussian RV with the mean 0 and the variance $\left(4\sigma_n^2 A_m^2 / \eta^2 P_t^2 \right) \| \boldsymbol{G}_j - \boldsymbol{G}_i \|^2$. Therefore, equation (20) can be reduced as

$$\overline{P}r \left(\hat{\boldsymbol{X}}_{\text{final}_i} \neq \boldsymbol{X}_i \right) = Q \left(\sqrt{\tau \delta K_l / 4 A_m^2} \right) \tag{21}$$

where $Q(\cdot)$ is Gaussian Q-function [31]. τ is the received signal to noise ratio (SNR) given by $\tau = \eta^2 P_t^2 / \sigma_n^2$. $\delta (2 \leq \delta \leq \xi)$ is the arithmetic mean of all possible times K_l, $K_l = \| \boldsymbol{g}_{i_a} - \boldsymbol{g}_{j_c} \|^2$ $(1 \leq \xi \leq N_t L, \text{ and } a \neq c)$.

By employing $Q(x) = 1/\pi \int_0^{\pi/2} \exp \left(-x^2 / 2 \sin^2 \theta \right) \mathrm{d}\theta$ [6], equation (21) can be rewritten as

$$\bar{P}r \left(\hat{\boldsymbol{X}}_{\text{final}_i} \neq \boldsymbol{X}_i \,|\, \rho \leq V_{\text{th}} \right) \\ = \frac{1}{\pi} \int_0^{\frac{\pi}{2}} F_B \left(-\tau \delta K_l / 8 A_m^2 \sin^2 \theta \mathrm{d}\theta \right) \tag{22}$$

where $F_B(\kappa) = \int_0^\infty f_B(\Gamma) \exp(\Gamma \kappa) \mathrm{d}\Gamma$ is the moment generating function (MGF) of variable B.

Considering each square term in the equation $K_l = \sum_{m=1}^{N_r} \left(g_{m i_a} - g_{m j_c} \right)^2$, it is the difference between two random variables that obey the EW distribution, equation (22) can be approximated by kernel density estimation (KDE) [6]

$$\bar{P}r \left(\hat{\boldsymbol{X}}_{\text{final}_i} \neq \boldsymbol{X}_i \,|\, \rho \leq V_{\text{th}} \right) \\ \approx \sum_{l=1}^{n_2} \frac{1}{n_2 \pi} \int_0^{\frac{\pi}{2}} M_{K_l} \left(-\tau \delta / 8 A_m^2 \sin^2 \theta \right) \mathrm{d}\theta \tag{23}$$

where $M_{K_l}(\kappa) = \exp\left(\mu_i\kappa + 1/2\,\varsigma^2\kappa^2\right)$, n_2 stands for a kernel size, μ_i and ς are the mean of Gaussian distributed variable and kernel estimator bandwidth, respectively.

Next, we calculate $Pr\left(\rho_e \leq V_{th}\right)$ in (17). The distinct cases of ρ_e are analyzed as follows.

a) If the N_t activated lasers indices in the signal matrix are all correct, such as $(\boldsymbol{x}_{s_1} = \hat{\boldsymbol{x}}_{s_1}, \ldots, \boldsymbol{x}_{s_i} = \hat{\boldsymbol{x}}_{s_i}, \ldots, \boldsymbol{x}_{s_{N_t}} = \hat{\boldsymbol{x}}_{s_{N_t}})$, then $\rho_{e_1} = \|\boldsymbol{x}_{s_1}(\boldsymbol{x}_{p_1} - \hat{\boldsymbol{x}}_{p_1})\|_F^2 + \cdots + \|\boldsymbol{x}_{s_i}(\boldsymbol{x}_{p_i} - \hat{\boldsymbol{x}}_{p_i})\|_F^2 + \cdots + \left\|\boldsymbol{x}_{s_{N_t}}\left(\boldsymbol{x}_{p_{N_t}} - \hat{\boldsymbol{x}}_{p_{N_t}}\right)\right\|_F^2 + \|\boldsymbol{n}\|_F^2$.

b) If there are two activated laser indices misestimated in the signal matrix, the rest are correct, such as $(\boldsymbol{x}_{s_1} = \hat{\boldsymbol{x}}_{s_1}, \ldots, \boldsymbol{x}_{s_i} \neq \hat{\boldsymbol{x}}_{s_i}, \boldsymbol{x}_{s_j} = \hat{\boldsymbol{x}}_{s_j}, \ldots, \boldsymbol{x}_{s_{N_t}} = \hat{\boldsymbol{x}}_{s_{N_t}})$, then get $\rho_{e_2} = \|\boldsymbol{x}_{s_1}(\boldsymbol{x}_{p_1} - \hat{\boldsymbol{x}}_{p_1})\|_F^2 + \cdots + \boldsymbol{x}_{s_i}\boldsymbol{x}_{p_i} - \|\hat{\boldsymbol{x}}_{s_i}\hat{\boldsymbol{x}}_{p_i}\|_F^2 + \left\|\boldsymbol{x}_{s_j}\boldsymbol{x}_{p_j} - \hat{\boldsymbol{x}}_{s_j}\hat{\boldsymbol{x}}_{p_j}\right\|_F^2 + \cdots + \|\boldsymbol{n}\|_F^2$.

Considering the orthogonality of $\boldsymbol{x}_s$, the misestimated activated laser indices appear in pairs. Accordingly, there will be four, six, etc. activated laser indices misestimated, in case of which, ρ_e and ρ_{e_2} have similar forms.

c) If the N_t activated lasers indices in the signal matrix are all wrong, such as $(\boldsymbol{x}_{s_1} \neq \hat{\boldsymbol{x}}_{s_1}, \ldots, \boldsymbol{x}_{s_i} \neq \hat{\boldsymbol{x}}_{s_i}, \ldots, \boldsymbol{x}_{s_{N_t}} \neq \hat{\boldsymbol{x}}_{s_{N_t}})$, then $\rho_{e_{nn}} = \|\boldsymbol{x}_{s_1}\boldsymbol{x}_{p_1} - \hat{\boldsymbol{x}}_{s_1}\hat{\boldsymbol{x}}_{p_1}\|_F^2 + \cdots + \|\boldsymbol{x}_{s_i}\boldsymbol{x}_{p_i} - \hat{\boldsymbol{x}}_{s_i}\hat{\boldsymbol{x}}_{p_i}\|_F^2 + \cdots + \|\boldsymbol{x}_{s_{N_t}}\boldsymbol{x}_{p_{N_t}} - \hat{\boldsymbol{x}}_{s_{N_t}}\hat{\boldsymbol{x}}_{p_{N_t}}\|_F^2 + \|\boldsymbol{n}\|_F^2$, where nn is the number of all possible cases in ρ_e.

Define $Z_1 = \boldsymbol{x}_{s_i}(\boldsymbol{x}_{p_i} - \hat{\boldsymbol{x}}_{p_i})$ and $Z_2 = \boldsymbol{x}_{s_i}\boldsymbol{x}_{p_i} - \hat{\boldsymbol{x}}_{s_i}\hat{\boldsymbol{x}}_{p_i}$. According to KDE method, Z_1 and Z_2 obey Gaussian distribution with means μ_{Z_1}, μ_{Z_2}. Then, ρ_e follows the non-central chi-square distribution with freedom degree $N_r N_t L$. Therefore, $Pr\left(\rho_e \leq V_{th}\right)$ can be given as

$$Pr\left(\rho_e \leq V_{th}\right) = \int_0^{\frac{V_{th}}{E[Z_{kk}]}} f_{\chi^2(N_t N_r L)}(x)\,dx, \quad 1 \leq kk \leq nn \tag{24}$$

Thus, $\mathrm{ABER}_{\rho_e \leq V_{th}}$ can be obtained by substituting (23) and (24) into (17).

A tight upper bound for the $\mathrm{ABER}_{\mathrm{MLSD}}$ can be written as

$$\mathrm{ABER}_{\mathrm{MLSD}} \leq \frac{1}{R2^R}\sum\sum\left[d_H\left(\boldsymbol{X}_i, \hat{\boldsymbol{X}}_{\mathrm{final}_i}\right)\right.$$
$$\left.\times \mathrm{APEP}\left(\boldsymbol{X}_i \to \hat{\boldsymbol{X}}_{\mathrm{final}_i}\right)\right] \tag{25}$$

where the $\mathrm{APEP}\left(\boldsymbol{X}_i \to \hat{\boldsymbol{X}}_{\mathrm{final}_i}\right)$ is

$$\mathrm{APEP}\left(\boldsymbol{X}_i \to \hat{\boldsymbol{X}}_{\mathrm{final}_i}\right)$$
$$= \bar{\mathrm{Pr}}\left(\eta P_t\left\|\boldsymbol{H}\hat{\boldsymbol{X}}_{\mathrm{final}_i}\right\|^2 - 2\boldsymbol{Y}^{\mathrm{T}}\boldsymbol{H}\hat{\boldsymbol{X}}_{\mathrm{final}_i}\right.$$
$$\geq \eta P_t\|\boldsymbol{H}\boldsymbol{X}_i\|^2 - 2\boldsymbol{Y}^{\mathrm{T}}\boldsymbol{H}\boldsymbol{X}_i\Big) \tag{26}$$

The derivation of $\mathrm{APEP}\left(\boldsymbol{X}_i \to \hat{\boldsymbol{X}}_{\mathrm{final}_i}\right)$ is similar to that of equations (18)–(23), and $\mathrm{APEP}\left(\boldsymbol{X}_i \to \hat{\boldsymbol{X}}_{\mathrm{final}_i}\right)$ is approximated as

$$\mathrm{APEP}\left(\boldsymbol{X}_i \to \hat{\boldsymbol{X}}_{\mathrm{final}_i}\right)$$
$$\approx \sum_{l=1}^{n_2}\frac{1}{n_2\pi}\int_0^{\frac{\pi}{2}} M_{K_l}\left(-\tau\delta/4A_m^2\sin^2\theta\right)d\theta \tag{27}$$

Finally, the ABER of the OSTPPM-IT-OMP system can be obtained by substituting the $\mathrm{ABER}_{\rho_e \leq V_{th}}$ and $\mathrm{ABER}_{\mathrm{MLSD}}$ into the (15).

IV. Simulation and Analysis

In this section, the performance of the OSTPPM-IT-OMP over EW turbulence channel is analyzed. The system parameters are simply marked by (N_t, N_r, L). And N_u denotes the number of activated lasers of GSPPM scheme. The simulation parameters and turbulence parameters [32] are shown in Table 2 and Table 3. Without special explanation, the simulation results are completed under strong AT.

Table 2 Simulation parameters

Parameter	Symbol	Value
Link distance (m)	d_L	1000
Wavelength (nm)	λ	785
Aperture size (mm)	D_A	25
Photoelectric conversion efficiency (A/W)	η	0.5
Kernel estimator bandwidth	ς	1/5000

Table 3 Turbulence parameters

Turbulence intensity	C_n^2 (m$^{-2/3}$)	α	β	$\wp$
Weak AT	7.2×10^{-15}	3.67	1.97	0.73
Moderate AT	5.0×10^{-14}	5.37	0.81	0.33
Strong AT	3.6×10^{-13}	5.5	0.74	0.29

Figure 3 shows the $Pr(\rho \leq V_{th})$ curves with different system parameters of N_t, N_r and L. It can be observed that with the increase of θ, the probability of the Euclidean distance between $\hat{\boldsymbol{X}}_{\mathrm{final}_i}$ and $\boldsymbol{X}_i$ falling within the V_{th} increases, which reduces search steps and computational complexity. For instance, in order to satisfy $Pr(\rho \leq V_{th}) > 0.9$, the range of θ is $\theta \geq 1.4$ in the (3,4,2)-OSTPPM-IT-OMP.

The BER performances of (3,4,2)-OSTPPM-IT-OMP with different θ are shown in Figure 4. It can be obtained from Figure 4 and equations (11) and (12), when $\theta = 1$, the OSTPPM-MLSD has about 0.2 dB performance gain in comparison to OSTPPM-IT-OMP at $\mathrm{BER} = 1 \times 10^{-3}$. While its computational complexity is about 85.47% more than that of OSTPPM-IT-OMP. When θ increases from 1 to 2, the OSTPPM-IT-OMP has about 3.8 dB performance loss at BER=1×10^{-3}, but its computational complexity decreases by about 2.7%. Obviously, a reasonable V_{th} can achieve optimal BER performance and significantly reduce computational complexity.
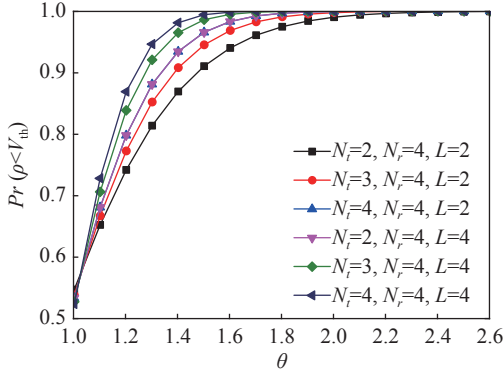
Figure 3 $Pr(\rho \leq V_{\text{th}})$ curves with different N_t, N_r and L.

Figure 4 BER performances of OSTPPM-IT-OMP with different θ.

Figure 5 Theoretical BER and simulation BER of the OSTPPM-IT-OMP scheme under different level of AT.
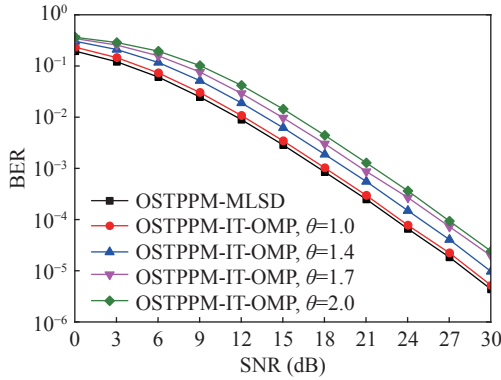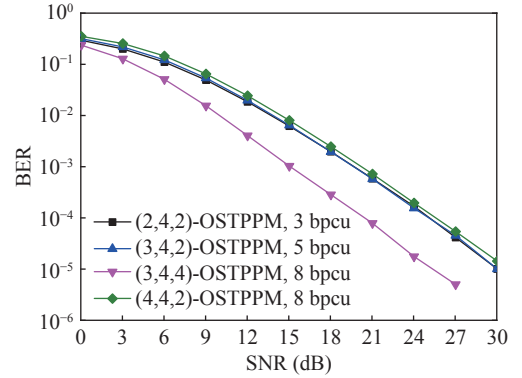

Figure 6 BER performances of OSTPPM-IT-OMP with different N_t and L.

The comparison of the simulation BER and theoretical BER results for (3,4,2)-OSTPPM-IT-OMP under the conditions of weak to strong AT are presented in Figure 5. The SNR of weak to strong AT is 33 dB at BER $= 1.8 \times 10^{-5}$, BER $= 1.5 \times 10^{-6}$ and BER $= 2 \times 10^{-6}$, respectively. The theoretical BER performance curves are in agreement with the simulation results at high SNR. It proved that the theoretical BER expression is derived correctly. In addition, the SNR of the OSTPPM-IT-OMP under weak, moderate and strong AT conditions is 24.1 dB, 20.25 dB, and 19.5 dB at BER $= 1 \times 10^{-3}$. Thus, the SNR of strong AT is almost 0.75 dB and 4.6 dB better than that under moderate AT and weak AT at BER $= 1 \times 10^{-3}$. The SNR of moderate AT is almost 3.85 dB better than that under weak AT at BER $=1 \times 10^{-3}$. The reason is that the more the difference, the more obvious the effect of diversity gain and the better is the performance. The scattering is more abundant under strong AT, so the more the differences among channels, the better is the BER performance.

The BER performance of OSTPPM-IT-OMP with different N_t and L are shown in Figure 6. As seen from the figure that with the increase of lasers, the BER performance decreases, while the TBS increase. For instance, the TBS of (4,4,2)-OSTPPM are nearly 3 times higher than that of (2,4,2)-OSTPPM, while it has about 0.7 dB performance loss at BER $= 1 \times 10^{-3}$. When the PPM order increases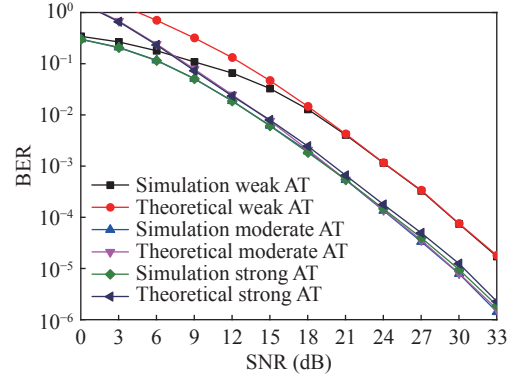, the TBS and BER performance of OSTPPM-IT-OMP are improved. The SNR of the (3,4,4)-OSTPPM performs 4.5 dB better than that of (3,4,2)-OSTPPM at BER $= 1 \times 10^{-3}$. And the TBS of (3,4,4)-OSTPPM increases 3 bpcu. Thus, compared with the increase of the lasers number, increasing the PPM order better improves the TBS and BER performance of the OSTPPM-IT-OMP.

Figure 7, Figure 8 and Table 4 compare the TBS, computational complexity, BER performance and bandwidth efficiency of OSTPPM versus SPPM [7] and GSPPM [10] ($N_u = 2$). With the same simulation parameters ($N_t, N_r = 4, L = 2$), the SNR of the OSTPPM scheme
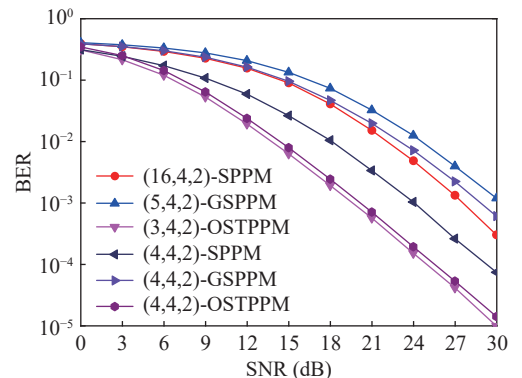

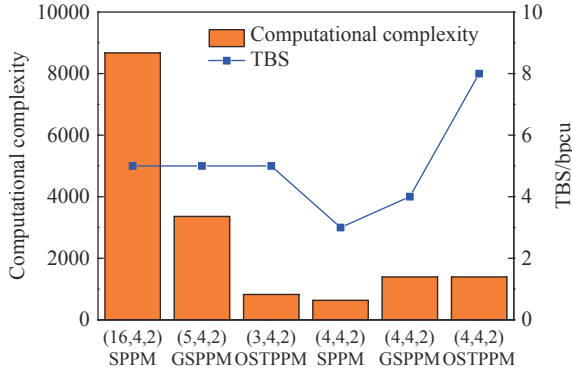**Figure 7** BER performances of different OSM schemes.

Figure 8 The computational complexity and TBS of different schemes.

outperforms SPPM and GSPPM by about 3.75 dB and 8.5 dB at BER $= 1 \times 10^{-3}$, respectively. At the same time, the TBS of OSTPPM is about twice higher than that of SPPM and GSPPM. But the computational complexity of the OSTPPM is about 54.53% and 0.14% higher than that of SPPM and GSPPM. With the TBS of 5 bpcu and $L = 2$, the SNR of (3,4,2)-OSTPPM outperforms (16,4,2)-SPPM and (5,4,2)-GSPPM by about 8 dB and 10.5 dB at BER $= 1 \times 10^{-3}$, respectively. At the same time, the

computational complexity of (3,4,2)-OSTPPM is about 90.47% and 75.4% lower than that of (16,4,2)-SPPM and (5,4,2)-GSPPM.

V. Conclusions

In this paper, an OSTPPM scheme is proposed to improve the TBS and BER performance. And the low-complexity IT-OMP algorithm fit for OSTPPM scheme is proposed. The computational complexity of IT-OMP algorithm near optimal detector is reduced about over 80% compared with MLSD. Using Monte Carlo simulation, we analyze the BER performance of the proposed scheme under different AT conditions, and discuss the effect of the number of lasers and PPM order on BER performance and TBS. As a result, increasing the PPM order better improves the BER performance and TBS. With the same simulation parameters, the SNR of (4,4,2)-OSTPPM-IT-OMP is 3.75 dB and 8.5 dB better than that of SPPM and GSPPM at BER $= 1 \times 10^{-3}$. With the same TBS, the computational complexity of (3,4,2)-OSTPPM-IT-OMP is reduced by 90.47% and 75.4% compared with (16,4,2)-SPPM and (5,4,2)-GSPPM. Therefore, OSTPPM-IT-OMP scheme has a better application prospect than SPPM and GSPPM schemes.

Table 4 TBS, computational complexity and bandwidth efficiency of different OSM schemes in [7], [10] and this paper

Modulation	TBS	Computational complexity	Bandwidth efficiency
SPPM-MLSD	$\log_2 N_t + \log_2 L$	$2^{\log_2 N_t + \log_2 L} \times$ $(2N_r N_t L + 2N_r L - 1)$	$(\log_2 N_t + \log_2 L)/L$
GSPPM-MLSD	$\left\lfloor \log_2 C_{N_t}^{N_u} \right\rfloor + N_u \log_2 L$	$2^{\left\lfloor \log_2 C_{N_t}^{N_u} \right\rfloor + N_u \log_2 L} \times$ $(2N_r N_t L + 2N_r L + N_t L - 1)$	$\left\lfloor \log_2 C_{N_t}^{N_u} \right\rfloor + (N_u \log_2 L)/L$
OSTPPM-IT-OMP	$\lfloor \log_2 (N_t!) \rfloor + N_t \log_2 L$	$2N_r N_t^2 L - N_t^2 L + N_r N_t +$ $\left(2N_r N_t^2 L + 2N_r N_t L - 1\right)\gamma$	$[\lfloor \log_2 (N_t!) \rfloor + N_t \log_2 L]/(N_t L)$

Acknowledgement

References

[1] P. W. Berenguer, P. Hellwig, D. Schulz, *et al.*, "Real-time optical wireless mobile communication with high physical layer reliability," *Journal of Lightwave Technology*, vol. 37, no. 6, pp. 1638–1646, 2019.

[2] Y. Y. Du, J. L. Chen, Y. M. Lei, *et al.*, "Performance analysis of nonlinear spatial modulation multiple-input multiple-output systems," *Digital Signal Processing*, vol. 115, article no. 103064, 2021.

[3] D. Y. Ma, N. Shlezinger, T. Y. Huang, *et al.*, "Spatial modulation for joint radar-communications systems: Design, analysis, and hardware prototype," *IEEE Transactions on Vehicular Technology*, vol. 70, no. 3, pp. 2283–2298, 2021.

[4] H. Albinsaid, K. Singh, S. Biswas, *et al.*, "Block deep neural network-based signal detector for generalized spatial modulation," *IEEE Communications Letters*, vol. 24, no. 12, pp. 2775–2779, 2020.

[5] A. Bhowal and R. S. Kshetrimayum, "Advanced optical spatial modulation techniques for FSO communication," *IEEE Transactions on Communications*, vol. 69, no. 2, pp. 1163–1174, 2021.

[6] T. Ozbilgin and M. Koca, "Optical spatial modulation over atmospheric turbulence channels," *Journal of Lightwave Technology*, vol. 33, no. 11, pp. 2313–2323, 2015.

[7] W. O. Popoola, E. Poves, and H. Haas, "Spatial pulse position modulation for optical communications," *Journal of Lightwave Technology*, vol. 30, no. 18, pp. 2948–2954, 2012.

[8] H. T. T. Pham and N. T. Dang, "Performance improvement of spatial modulation-assisted FSO systems over Gamma–Gamma fading channels with geometric spreading," *Photonic Network Communications*, vol. 34, no. 2, pp. 213–220, 2017.

[9] C. Abou-Rjeily and G. Kaddoum, "Optical spatial modulation for FSO IM/DD communications with photon-counting receivers: Performance analysis, transmit diversity order and aperture selection," *IEEE Journal on Selected Areas in Communications*, vol. 37, no. 9, pp. 2053–2068, 2019.

[10] H. G. Olanrewaju, J. Thompson, and W. O. Popoola, "Generalized spatial pulse position modulation for optical wireless communications," in *Proceedings of the 2016 IEEE 84th Vehicular Technology Conference (VTC-Fall)*, Montreal, QC, Canada, pp.1–5, 2016.

[11] S. P. Alaka, T. L. Narasimhan, and A. Chockalingam, "Generalized spatial modulation in indoor wireless visible light

communication," in *Proceedings of the 2015 IEEE Global Communications Conference*, San Diego, CA, USA, pp.1–7, 2015.

[12] C. Rajesh Kumar and R. K. Jeyachitra, "Power efficient generalized spatial modulation MIMO for indoor visible light communications," *IEEE Photonics Technology Letters*, vol. 29, no. 11, pp. 921–924, 2017.

[13] E. E. Elsayed and B. B. Yousif, "Performance enhancement of hybrid diversity for M-ary modified pulse-position modulation and spatial modulation of MIMO-FSO systems under the atmospheric turbulence effects with geometric spreading," *Optical and Quantum Electronics*, vol. 52, no. 12, article no. 508, 2020.

[14] E. E. Elsayed and B. B. Yousif, "Performance enhancement of the average spectral efficiency using an aperture averaging and spatial-coherence diversity based on the modified-PPM modulation for MISO FSO links," *Optics Communications*, vol. 463, article no. 125463, 2020.

[15] E. E. Elsayed, B. B. Yousif, and M. Singh, "Performance enhancement of hybrid fiber wavelength division multiplexing passive optical network FSO systems using M-ary DPPM techniques under interchannel crosstalk and atmospheric turbulence," *Optical and Quantum Electronics*, vol. 54, no. 2, article no. 116, 2022.

[16] S. Magidi and A. Jabeena, "Analysis of multi-pulse position modulation free space optical communication system employing wavelength and time diversity over Malaga turbulence channel," *Scientific African*, vol. 12, article no. e00777, 2021.

[17] E. E. Elsayed, A. G. Alharbi, M. Singh, *et al.*, "Investigations on wavelength-division multiplexed fibre/FSO PON system employing DPPM scheme," *Optical and Quantum Electronics*, vol. 54, no. 6, article no. 358, 2022.

[18] H. Ullah, M. Sohail, and M. Bokhari, "Dynamic range of LED in optical OFDM for PAPR performance analysis," *Optical and Quantum Electronics*, vol. 54, no. 11, article no. 742, 2022.

[19] S. M. Hameed, S. M. Abdulsatar, and A. A. Sabri, "Performance enhancement for visible light communication based ADO-OFDM," *Optical and Quantum Electronics*, vol. 53, article no. 339, 2021.

[20] A. Jaiswal, M. R. Bhatnagar, P. Soni, *et al.*, "Differential optical spatial modulation over atmospheric turbulence," *IEEE Journal of Selected Topics in Signal Processing*, vol. 13, no. 6, pp. 1417–1432, 2019.

[21] H. Q. Wang, Y. C. Mao, Y. Zhang, *et al.*, "Differential optical spatial modulation with pulse position modulation over atmospheric turbulence," *Optical Engineering*, vol. 59, article no. 096109, 2020.

[22] A. Stavridis and H. Haas, "Performance evaluation of space modulation techniques in VLC systems," *in Proceedings of the 2015 IEEE International Conference on Communication Workshop (ICCW 2015)*, London, UK, pp. 1356–1361, Jun. 2015.

[23] H. Q. Wang, L. H. Song, M. H. Cao, *et al.*, "Compressed sensing detection of optical spatial modulation signal in turbulent channel," *Optics and Precision Engineering*, vol. 26, no. 11, pp. 2669–2674, 2018. (in Chinese)

[24] H. Q. Wang, W. B. Hou, Q. B. Peng, *et al.*, "Step-by-step classification detection algorithm of SPPM based on K-means clustering," *Journal on Communications*, vol. 43, no. 1, pp.

161–171, 2022. (in Chinese)

[25] Y. Zhang, H. Q. Wang, X. M. Ma, *et al.*, "Performance analysis and optimal detector of wireless optical space-time shift keying over the Gamma-Gamma turbulence channel," *Applied Optics*, vol. 60, no. 12, pp. 3501–3509, 2021.

[26] C. Chen, L. Zeng, X. Zhong, *et al.*, "Deep learning-aided OFDM-based generalized optical quadrature spatial modulation," *IEEE Photonics Journal*, vol. 14, no. 1, article no. 7302306, 2022.

[27] H. S. Khallaf, A. E. Elfiqi, H. M. H. Shalaby, *et al.*, "On the performance evaluation of LQAM-MPPM techniques over exponentiated Weibull fading free-space optical channels," *Optics Communications*, vol. 416, pp. 41–49, 2018.

[28] A. Jaiswal, M. R. Bhatnagar, and V. K. Jain, "Partially informed transmitter-based optical space shift keying under atmospheric turbulence," *IEEE Transactions on Wireless Communications*, vol. 18, no. 8, pp. 3781–3796, 2019.

[29] R. Barrios and F. Dios, "Exponentiated Weibull model for the irradiance probability density function of a laser beam propagating through atmospheric turbulence," *Optics & Laser Technology*, vol. 45, pp. 13–20, 2013.

[30] B. Hassibi and H. Vikalo, "On the sphere-decoding algorithm I. Expected complexity," *IEEE Transactions on Signal Processing*, vol. 53, no. 8, pp. 2806–2818, 2005.

[31] S. Fang, L. Li, S. Hu, *et al.*, "Layered space shift keying modulation over MIMO channels," *IEEE Transactions on Vehicular Technology*, vol. 66, no. 1, pp. 159–174, 2017.

[32] R. Barrios, "Exponentiated Weibull fading channel model in free-space optical communications under atmospheric turbulence," *Ph. D. Dissertation, Department of Signal Theory and Comunications, Universitat Politècnica de Catalunya (BarcelonaTech)*, Spain, pp. 116–118, 2013.

Yue ZHANG was born in 1994. She received the B.E. degree in information and computing science from Nanjing University of Posts and Telecommunications, Nanjing, China, in 2016, and the Ph.D. degree in manufacturing information system from Lanzhou University of Technology, Lanzhou, China, in 2021. Currently, she is working as a Lecturer at School of Computer and Communication, Lanzhou University of Technology. Her research interests include wireless optical communication and MIMO technology.
(Email: zyue940209@163.com)

Huiqin WANG was born in 1971. She received the B.E. degree in communication engineering from Lanzhou Jiaotong University, Lanzhou, China, in 1996, and the Ph.D. degree in microelectronics and solid state electronics from Xi'an University of Technology, Xi'an, China, in 2011. Currently, she is working as a Professor at School of Computer and Communication, Lanzhou University of Technology. Her research interests include the theory and technology of wireless optical communications.
(Email: whq1222@lut.edu.cn)